Modeling the wave power distribution and characteristics of plasmaspheric hiss

J. Bortnik,[1] L. Chen,[1] W. Li,[1] R. M. Thorne,[1] N. P. Meredith,[2] and R. B. Horne[2]

Received 19 May 2011; revised 9 September 2011; accepted 3 October 2011; published 10 December 2011.

[1] We simulate the spatial and spectral distributions of plasmaspheric hiss using a technique that involves extensive ray tracing. The rays are injected in the equatorial chorus source region outside the plasmasphere, are power weighted as a function of *L*-shell, frequency, and wave normal angle, so as to represent the chorus source distribution, and are propagated throughout the simulation domain until the power in each ray is effectively extinguished due to Landau damping. By setting up a large number of virtual observatories, the rays passing each observation location are counted, and a distribution is constructed. Our simulated plasmaspheric hiss spectrum reproduces the main observed features, including the lower and upper frequency cutoffs, the behavior of the bandwidth as a function of *L*-shell, the spatial extent, and even the two-zone structure of hiss, although the intensity is lower than observed. The wave normal distribution shows that at high latitudes, the wave normals are predominantly oblique, but near the equator, the wave normal distribution can be either predominantly field-aligned (lower *L* shells), or be bimodal, having a maximum in the field-aligned direction, and another maximum at very oblique angles, comprised of those rays that have broken out of their cyclical trajectories. This distribution of wave normals seems to reconcile the apparently contradictory observations that have been reported previously.

Citation: Bortnik, J., L. Chen, W. Li, R. M. Thorne, N. P. Meredith, and R. B. Horne (2011), Modeling the wave power distribution and characteristics of plasmaspheric hiss, *J. Geophys. Res.*, *116*, A12209, doi:10.1029/2011JA016862.

1. Introduction

[2] Plasmaspheric hiss (PH) is a structureless, band-limited, natural emission that has been commonly observed by high-altitude satellites ever since its discovery in the late 1960's [*Taylor and Gurnett*, 1968; *Dunckel and Helliwell*, 1969; *Russell et al.*, 1969; *Thorne et al.*, 1973]. As its name suggests, PH is generally confined to the plasmasphere and high-density regions such as plasmaspheric plumes [*Chan and Holzer*, 1976; *Cornilleau-Wehrlin et al.*, 1978; *Hayakawa et al.*, 1986; *Parrot and Lefeuvre*, 1986], and possibly a high-latitude dayside plume region [*Russell et al.*, 1969]. Previous studies have shown that PH typically occurs in the frequency range from ~200 Hz to a few kHz, although it is typically found below ~2 kHz [*Hayakawa and Sazhin*, 1992], with broadband amplitudes that are controlled by the level of geomagnetic activity, and range from ~10 pT during quiet times, to >100 pT during active periods [*Smith et al.*, 1974; *Thorne et al.*, 1974, 1977; *Meredith et al.*, 2004]. Although PH occurs at essentially all magnetic local times (MLT) and latitudes within the plasmasphere, there is nevertheless a pronounced MLT asymmetry in wave power, with dayside values being roughly an order of magnitude larger than those on the nightside [*Meredith et al.*, 2004, 2006a].

[3] Figure 1 shows wave electric field data from the CRRES satellite, and illustrates many of the common properties of PH listed above. At ~1010 UT CRRES enters the dayside plasmasphere during a period of disturbed geomagnetic conditions (Figure 1, top) and begins to observe intense PH spanning ~200 Hz to 3 kHz, extending all the way from the plasmapause to the lowest *L*-shells sampled by CRRES (albeit at much reduced intensities). Unlike the chorus emissions observed outside the plasmasphere, the PH spectrum does not scale with the equatorial gyrofrequency f_{ce} and in fact the PH bandwidth is seen to gradually diminish with decreasing *L*. We also point out the two zones of high intensity, separated near $L \sim 3.7$ which was noted previously (although at lower *L*) [*Tsurutani et al.*, 1975].

[4] Not long after its discovery, PH was recognized as playing a key role in controlling the structure and dynamics of the Earth's radiation belts. Specifically, resonant pitch angle scattering of energetic electrons by PH largely accounts for the formation of the slot region that separates the inner ($1.3 < L < 2.5$) and outer ($3 < L < 7$) radiation belts [*Lyons et al.*, 1972; *Lyons and Thorne*, 1973; *Albert*, 1994; *Abel and Thorne*, 1998a, 1998b; *Meredith et al.*, 2009], and largely controls the gradual decay of energetic outer-belt electrons during quiet times [*Meredith et al.*, 2006b; *Summers et al.*, 2007; *Lam et al.*, 2007]. In addition, PH is often observed in plumes, which could play a further role in outer radiation-belt dynamics [*Summers et al.*, 2008].

[1]Department of Atmospheric and Oceanic Sciences, University of California, Los Angeles, California, USA.
[2]British Antarctic Survey, Cambridge, UK.

0148-0227/11/2011JA016862

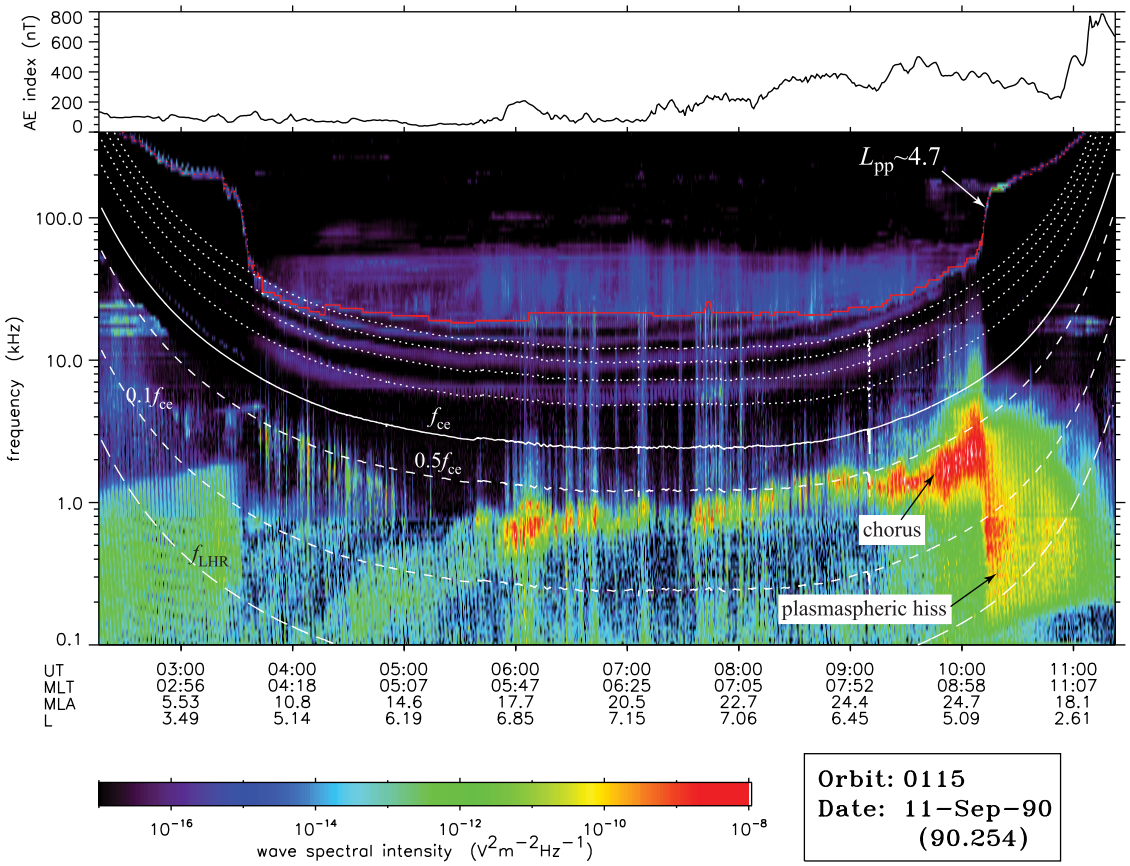

Figure 1. (bottom) An example of whistler mode chorus and plasmaspheric hiss observed on the CRRES satellite on September 11, 1990. (top) The AE index.

[5] A critical factor in quantifying which population of particles will be scattered, as well as the scattering rate of those particles, is the distribution of the PH wave power spatially (i.e., as a function of L and latitude, λ), and as a function of wave normal angle ψ. As an example, we plot the resonant energy, E_{res}, of loss cone electrons (assumed lost at an altitude of 100 km) as a function of ψ in Figure 2, parameterized by L, λ, and m (resonant harmonic number) based on the well-known resonance condition:

$$\omega - k_{\parallel} v_{\parallel} = m\Omega/\gamma \qquad (1)$$

where ω is the angular wave frequency, $k_{\parallel}$ and $v_{\parallel}$ are the components of the wave number k and particle velocity v parallel to the background magnetic field, Ω is the electron gyrofrequency and $\gamma = (1 - v^2/c^2)^{-1/2}$. Here, we have assumed a dipole variation for the magnetic field, a typical PH wave frequency of $f = 700$ Hz, and an equatorial electron number density modeled after *Carpenter and Anderson* [1992] and extended to off-equatorial locations using the simple expression: $N_e(\lambda) = N_e^{eq} \cos^{-2}\lambda$ [*Denton et al.*, 2002]. The first order ($m = 1$) cyclotron resonant energies exhibit tremendous variation as a function of L, λ, and ψ. For example, field-aligned ($\psi = 0°$) waves can affect particles with energies of ~1 − 10 MeV at $L = 2$, but these energies shift to much lower values, namely ~20 − 700 keV at $L = 4$. Perhaps more dramatic though, is the roughly 2-orders of magnitude variation in E_{res} over the range of ψ. For instance, at the equator at $L = 3$, E_{res} varies from ~100 keV near $\psi = 0°$ to ~10 MeV near $\psi = 89°$. Clearly, determining where the PH power is concentrated in L, λ, and ψ critically affects the population of electrons that will be scattered. In addition to controlling the resonant energy of electrons, the distribution of the wave power also affects the scattering rates themselves. For instance, calculating the lifetime of 1 MeV electrons at $L = 3$ under disturbed conditions, *Meredith et al.* [2007] found that the lifetime was <1 day when the wave power was assumed to be concentrated around small ψ, but increased to >100 days when it was assumed to be concentrated near $\psi = 80°$.

[6] Despite its recognized importance, the spatial distribution of PH wave power as a function of wave normal has been notoriously difficult to obtain experimentally. For one thing, the majority of techniques that compute the wave normal angle of a propagating wave assume *a priori* that the wave is planar, and essentially solve the divergence equation $\mathbf{k} \cdot \mathbf{B} = 0$ using a variety of approaches [e.g., *Means*, 1972; *McPherron et al.*, 1972; *Samson*, 1973; *Samson and Olsen*, 1980; *Santolík et al.*, 2003a]. In the case of PH, the wave is known to be broadband and structureless, implying that it is composed of numerous superposed plane waves, and thus assuming that only a single wave exists is incorrect. To address this shortcoming, *Storey and Lefeuvre* [1974, 1979, 1980] introduced the Wave Distribution Function (WDF) method whose aim is to identify a function, $G(f, \psi, \phi)$ (where ϕ is the azimuthal angle of $\mathbf{k}$), which describes how the wave

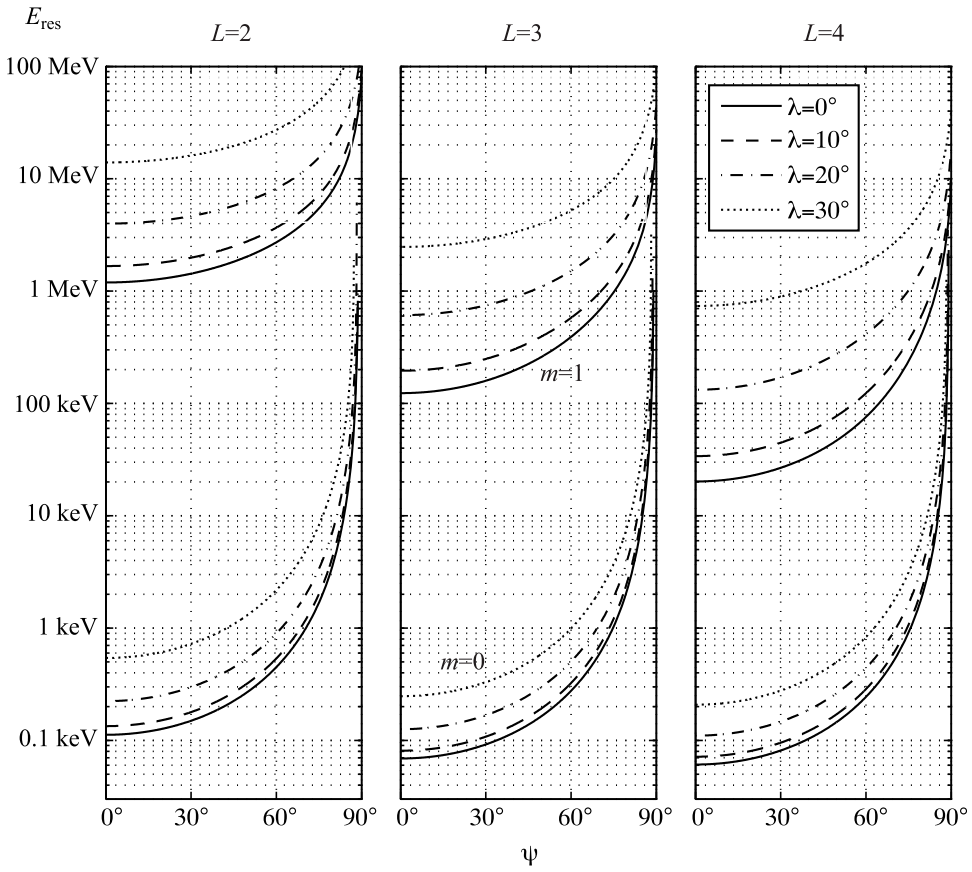

Figure 2. The resonant energy of loss cone electrons interacting with a whistler wave at the Landau (m = 0) and fundamental (m = 1) gyroresonance at L = 2, 3, and 4. The wave frequency is f = 700 Hz, and energy is shown as a function of wave normal angle, parameterized by the interaction latitude λ.

power at a given point in space is distributed as a function of the wave normal angles, at a given wave frequency *f*. *G* usually consists of a summation of a number of functions (e.g., Gaussians or simple 'tiles'), whose parameters are found iteratively in such a way as to optimally fit the measured data (e.g., see *Santolík and Parrot* [2000] for a comparison of a few fitting functions). Using the WDF method, a few seemingly mixed results were obtained. *Santolík et al.* [2001] reported that well within the plasmasphere, most of the hiss near the equator was propagating roughly along the field line, with a few instances where a second population of (weaker) waves at high wave normals appeared. *Storey et al.* [1991] observed that most of the PH waves were propagating obliquely at high latitudes, but that on one of the passes near the equator, some wave energy was seen at small wave normal angles. *Hayakawa et al.* [1986] found the presence of 2 different groups of waves at an equatorial region 0.3–0.5 R_e within the plasmapause, one group having medium wave normals $\psi = 20° - 60°$, and the other having large wave normals, $\psi = 70° - 80°$. At high latitudes, only large wave normal angles in the range $\psi = 80° - 85°$ were found. Finally, in their comprehensive review, *Hayakawa and Sazhin* [1992] reported that sometimes investigators found low wave normal angles, $\psi < 20°$, but in other cases large values of ψ were predominant, even going all the way to 90°.

[7] The aim of the present paper is to extend the model of PH presented by *Bortnik et al.* [2008], which treats whistler mode chorus as the principal source of PH. This is somewhat reversed to the view that chorus emissions are triggered from a hiss band [e.g., *Koons*, 1981], but a rare conjunction event linking the two emissions has indeed shown that it is the PH intensity that lags by a few seconds behind the chorus waves, in agreement with model predictions [*Bortnik et al.*, 2009]. On the other hand, previous studies have shown that chorus propagating to low altitudes is often observed as 'structured hiss' [*Santolík et al.*, 2006], and exhibits a wave normal distribution [*Santolík and Parrot*, 1999, Figure 2] which is very similar to our low altitude ray tracing results [see, e.g., *Bortnik et al.*, 2008, Figure 1].

[8] By properly weighting and ray tracing numerous rays from the chorus source region, into the plasmasphere, a distribution of PH can be constructed as a function of f, ψ, L, and λ. In section 2 we introduce the methodology required to construct such distributions, and in section 3 we present the initial set of results for a single plasmaspheric model. We discuss the implication of this work and state our primary conclusions in section 4.

2. Methodology

[9] The overarching goal of the present work is to construct the distribution of wave power of PH at any location

within the plasmasphere, and to be able to view this distribution in a way which can be compared with data, for instance, as a function of frequency and L-shell (comparable to Figure 1). In order to do so, we must specify a realistic model of the chorus wave power at its source, and using ray tracing, propagate this wave power away from its source region, along the path of the rays. By keeping track of the rays passing a certain observation location in the plasmasphere, and properly adding the power of these rays into a set of bins distributed in ψ and f, we can reconstruct the distribution of the PH wave power at any prescribed location. We then move the observation location systematically through space, and in this way build up the global spatial distribution of wave power in any desired region.

2.1. Representing the Chorus Source Region

[10] Chorus waves typically occur as a series of short (~0.1 sec), coherent bursts of wave power that are confined to two frequency bands [*Burtis and Helliwell*, 1969] that scale with the equatorial gyrofrequency f_{ce}: the lower band ($f/f_{ce} \sim 0.1 - 0.5$, with a peak at $f \sim 0.34 f_{ce}$), and the upper band ($f/f_{ce} \sim 0.5 - 0.7$, with a peak at $f \sim 0.53 f_{ce}$) [e.g., *Burtis and Helliwell*, 1976]. An example of a typical lower-band chorus observation on the CRRES satellite is shown in Figure 1, where the chorus is seen to be confined to slightly below $0.5 f_{ce}$, and becomes enhanced in association with elevated geomagnetic activity (e.g., Figure 1 (top) showing the AE index). As shown in Figure 1, the source region of chorus waves lies in the low-density plasmatrough [e.g., *Meredith et al.*, 2003; *Santolík et al.*, 2005b; *Li et al.*, 2009], with wave power extending from the plasmapause to $L > 10$ [*Li et al.*, 2009]. Chorus waves show MLT dependence, and usually occur in the night, dawn, and day sectors, with a significantly lower occurrence in the dusk sector [*Meredith et al.*, 2001, 2003; *Li et al.*, 2009]. Observations have shown that chorus consistently propagates away from the equator, implying that the generation region is located near the equator [*LeDocq et al.*, 1998; *Lauben et al.*, 1998, 2002; *Parrot et al.*, 2003; *Santolík et al.*, 2005a, 2005b]. Studies of the wave normal distribution of chorus near the source region indicate that wave normals can take on a range of values, from predominantly field aligned [*Burton and Holzer*, 1974; *Goldstein and Tsurutani*, 1984; *Hayakawa et al.*, 1984; *Santolík et al.*, 2003b], to ring-like [*Santolík et al.*, 2009], and oblique [*Lefeuvre and Helliwell*, 1985; *Hayakawa et al.*, 1990; *Lauben et al.*, 2002; *Tsurutani et al.*, 2009]. A recent analysis of an extensive set of observations indicates that for the most intense and common chorus forms (lower-band, rising elements), the wave normals are generally small and clustered around the field-aligned direction [*Li et al.*, 2011], which agrees with the general expectations of linear growth theory [*Kennel*, 1966].

[11] In order to model the chorus source region to be consistent with the characteristics described above, we launch rays over a range of L-shells ranging from just outside the outer edge of the plasmapause at $L = 5.0$, to $L = 7.6$ (where rays can no longer access the plasmasphere), spaced at intervals of $0.1L$ giving a total of 29 equatorial injection points, L_i (where the subscript i denotes the initial value). At each L_i, we launch a set of frequencies to represent the entire lower band, $f/f_{ce} = 0.05 - 0.5$, spaced at intervals of $0.05 f_{ce}$, giving a total of 10 frequency components, f_i. At each equatorial injection point, and for each wave frequency, we launch rays with a range of wave normal angles ψ_i, from $-\psi_{res}$ to $+\psi_{res}$ (pointing northward), and $180° - \psi_{res}$ to $180° + \psi_{res}$ (pointing southward), where ψ is measured clockwise from the direction of $\mathbf{B}_0$ (negative angles indicating that the rays are directed toward lower L-shells), and ψ_{res} is the resonance cone angle, beyond which propagation is not possible in a cold plasma, spaced at intervals of 0.5°. The number of rays launched at every (L_i, f_i) varies because ψ_{res} is frequency-dependent, but is typically in the range 240–350. A rough calculation shows that we use a total of ~100,000 rays to represent the chorus source region. The cold plasma density, chorus wave intensities, and suprathermal fluxes are all selected at MLT = 10, to represent the most probable and most intense region of chorus and hiss [e.g., *Dunckel and Helliwell*, 1969, Figure 7]. This MLT region also avoids the location of large azimuthal density gradients such as the plasmaspheric drainage plume, which would necessitate 3D ray tracing [*Chen et al.*, 2009]. Further details of the various models used in the ray tracing and damping calculations, as well as example raypaths are given by *Bortnik et al.* [2011].

[12] The rays are intensity-weighted at their injection points to represent the entire chorus region. The weighting is divided into 3 individual components representing the dependence on ψ, f, and L-shell, respectively. The wave normal weighting is chosen to maximize power in the field-aligned direction following several current models [*Glauert and Horne*, 2005; *Albert*, 2005], and is given as:

$$P_i \propto \exp\left(\frac{-(X_i - X_m)^2}{X_w^2}\right) \tag{2}$$

where $X_i = \tan(\psi_i)$, $X_m = \tan(0°)$, and $X_w = \tan(45°)$. Similarly, the frequency weighting is chosen as:

$$P_i \propto \exp\left(\frac{-(f_i - f_m)^2}{f_w^2}\right) \tag{3}$$

where all frequencies are understood to be normalized to f_{ce}, $f_m = 0.25$, and $f_w = 0.15$, consistent with values typically observed on the dayside [e.g., *Bortnik et al.*, 2007; *Li et al.*, 2007].

[13] The distributions in X and f are normalized such that:

$$A_L \iint \exp\left(\frac{-(X_i - X_m)^2}{X_w^2}\right) \exp\left(\frac{-(f_i - f_m)^2}{f_w^2}\right) dX\, df = 1 \tag{4}$$

where A_L is the L-dependent normalization factor.

[14] The distribution of wave intensity as a function of L is modeled roughly after the distribution of *Li et al.* [2009] at low latitudes, in the MLT region between 0900 and 1100 for moderately active to active conditions [e.g., *Li et al.*, 2009, Figure 2a]. This distribution peaks at $L \sim 7 - 8$, and ranges from ~10 pT near the plasmapause, to ~100 pT at $L = 7$, and is expressed as:

$$B_w(L_i) = 100 \exp\left(\frac{-(L_i - L_m)^2}{L_w^2}\right) \tag{5}$$

where $L_m = 7$ and $L_w = 0.15$, and B_w is in units of pT.

[15] As a result, each ray is weighted with an initial intensity given by:

$$P_i(L_i, f_i, \psi_i) = A_L \left[100 \exp\left(\frac{-(L_i - L_m)^2}{L_w^2} \right) \right]^2 \exp\left(\frac{-(f_i - f_m)^2}{f_w^2} \right) \cdot \exp\left(\frac{-(X_i - X_m)^2}{X_w^2} \right) \Delta L \Delta f \Delta X \quad (6)$$

[16] Each ray is then ray traced and the path-integrated Landau damping is calculated together with a geometric contraction factor to represent the convergence of magnetic field lines. In these simulations, wave growth is omitted because the process of chorus wave excitation becomes very rapid near the source leading to nonlinear effects such as frequency-shifting and saturation, that cannot be handled by linear theory. The ray is terminated when it reaches 1% of its initial power for the last time on its trajectory, leaves the system, or the refractive index $n > 500$, indicating that the assumptions of cold-plasma theory are no longer strictly valid (this occurs for a very small number of rays, and is discussed further by *Bortnik et al.*, 2011). The time at the termination of the ray will be referred to as the lifetime of the ray below.

[17] Figure 3 shows a few selected rays launched at $L_i = 6$, $f = 0.1 f_{ce}$, in the range $\psi_i = -67°$ to $-47°$, each displayed for the duration of its lifetime (noted above each plot). This particular range of ψ_i is chosen because it is these rays that are able to avoid the large Landau damping near the chorus source region, and propagate all the way to the plasmasphere, where they merge into plasmaspheric hiss. The lifetimes are typically in the range of 10's of seconds, and the raypaths exhibit a wide range of morphologies, often differing from each other dramatically even though they are almost identical and are separated in initial conditions by only a few degrees in ψ_i. We also note that even though we have only chosen a single L_i and f_i value, and have chosen a relatively narrow slice of ψ_i, the resulting raypaths are nevertheless seen to fill virtually the entire plasmasphere, from the plasmapause to $L < 2$.

2.2. Representing the Wave Observation Locations

[18] We now aim to collect all the ray power from rays passing a certain observation location, which we shall refer to as the 'target' (denoted by the subscript t hereafter). The target has a certain location given by (L_t, λ_t), and a certain half-width in L, ΔL_t (remembering that MLT is fixed at 10). Focusing on one raypath at a time, we traverse the entire raypath and search for instances when the ray trajectory crosses λ_t, and is simultaneously within the range [$L_t - \Delta L_t$, $L_t + \Delta L_t$]. If this condition is satisfied, we extract the local wave normal of the ray at the location of the target, ψ_0 and the local intensity of the ray, $P_0 = GP_i(L_i, f_i, \psi_i)$ (where G is the path-integrated Landau damping and geometric factor, from the launch location to the target point, the latter introduced to account for the contraction of magnetic field lines in an azimuthally symmetric magnetic field [*Bortnik et al.*, 2011]). The wave distribution is then updated by adding P_0 into the appropriate wave normal bin. In our case, the wave normal distribution is discretized into $\Delta\psi_t = 10°$ wide bins, that range from $\psi_t = -180°$ to $+180°$. This procedure is repeated for every ray, traversing the range of f_i and ψ_i at each L_i.

[19] Since the ray frequencies at this point are still normalized to f_{ce}, the final step in the process is to resample the wave intensity onto a uniform, absolute frequency grid. For our purposes we use a frequency range spanning $f_{abs} = 0 - 10$ kHz, with interval spacing at every 10 Hz. In the interpolation process, it is important to preserve the total integrated power in moving from the normalized f to the absolute f distribution.

[20] In practice, we distribute our targets over the range $L_t = 1.2$ to 7, and $\lambda_t = -80°$ to $+80°$, with interval spacing of $0.1L$, and 2° respectively, thus covering the entire inner magnetosphere (in a meridional plane). For every raypath, we search for target crossing in the entire domain, and after all the rays from a single L_i have been examined, the distribution is resampled, at each target location, onto the absolute f grid discussed above. This operation necessarily needs to be performed for each L_i individually, because the absolute frequencies that the rays are normalized to (f_{ce}) vary with L.

[21] In many ways, this procedure is analogous to the generation of synthetic spectrograms introduced by *Bortnik et al.* [2003] in the analysis of lightning-generated whistlers, but in the present case we do not keep track of the temporal evolution of the wave power, but instead we bin the wave normal distribution.

[22] We should note that we have introduced a minor extension of the simple binning method described above in order to represent that rays have a certain 'thickness'. Instead of simply adding the wave power P_0 into the appropriate (L_t, λ_t, ψ_t) bin, we divide the wave power in proportion to its proximity to the bin-centers of two adjacent bins, in both L_t and ψ_t. For instance, if the ray crossed the target at an L value that was L_0, and not precisely at L_t, then the fraction:

$$\frac{P}{P_0} = \frac{\Delta L_t - |L_t - L_0|}{\Delta L_t} \quad (7)$$

would be added to that particular bin, where $\Delta L_t = 0.25$ (and the remainder of the power added to the adjacent bin). The power is divided in a similar way among the ψ_t bins. Since each ray is infinitely thin, the above operation is intended to mimic a certain width inherent in the ray, which is the case in the physical situation. This is achieved essentially by reversing the physical situation (which has a satellite as a point observation, and the wave having a finite width), but obtaining the same result.

[23] After all the rays from all the L_i are traversed, the distributions are divided by ΔL_t and $\Delta\psi_t$, such that the resultant intensity is expressed in units of $pT^2/Hz/deg$.

3. Results

[24] Using the procedure outlined in section 2, we produce the wave distribution $P_w(L_t, \lambda_t, f_t, \psi_t)$ which we will examine in this section. Figure 4 shows the distribution of wave power as a function of L-shell and f on the equatorial plane, i.e., $P_w(L_t, \lambda_t = 0°, f_t)$, integrated over the entire wave normal range of ψ_t. The grey vertical block in Figures 4a and 4b represents the plasmapause from its inner edge at $L_{pp} = 4.5$

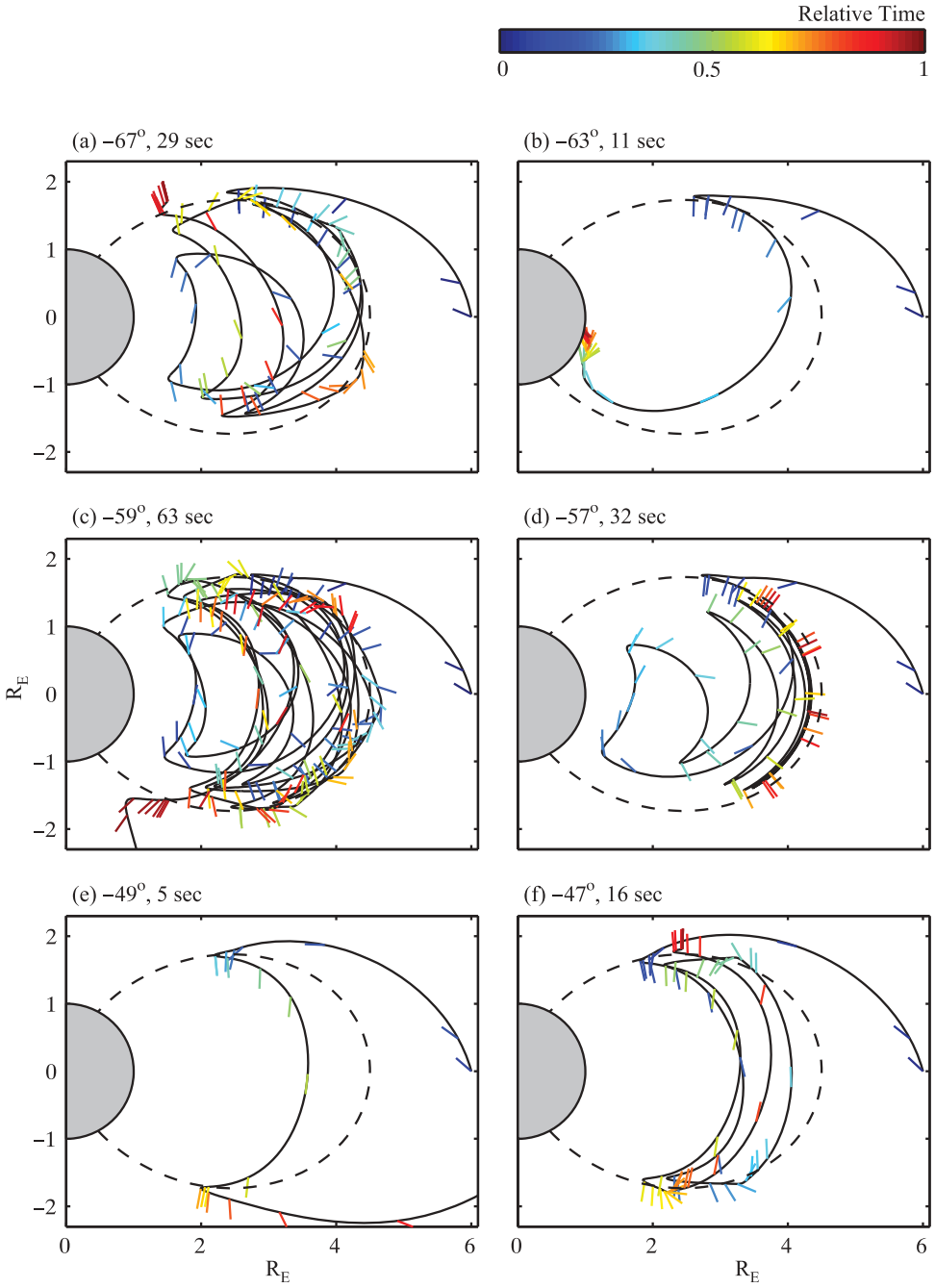

Figure 3. (a–f) Raypaths of 6 selected rays launched at $\lambda_0 = 0°$, $L = 6$ showing the evolution of whistler mode chorus waves into plasmaspheric hiss. Plots are labeled with the initial wave normal angle of the ray and its lifetime. The short line segments attached to each ray denote the local wave normal direction, and their color indicates the time elapsed relative to their lifetimes (shown on the common color scale). The dashed line indicates the location of the inner edge of the plasmapause, $L_{pp} = 4.5$.

to its outer edge at $L = 4.8$, and delineates the chorus source region which has been prescribed at $L > 5$ (as described above), from the PH region inside the plasmasphere, which has been calculated using the ray tracing procedure. The PH region in Figure 4b shows lower and upper frequency cutoffs at $f \sim 200$ Hz and $f \sim 2$ kHz respectively, and extends all the way from the plasmapause to $L < 2$, albeit at lower power. Both of these properties are in excellent agreement with observed values for PH.

[25] In order to better compare the chorus and hiss intensities, we have integrated the wave power in Figure 4b with respect to frequency (i.e., column-wise) and show the resulting wave amplitude as a function of L in Figure 4a as the blue curve, together with the electron number density for reference. We also show the prescribed wave amplitudes for the chorus source as the red-dashed curve for comparison, and as a check that our binning and interpolation procedure

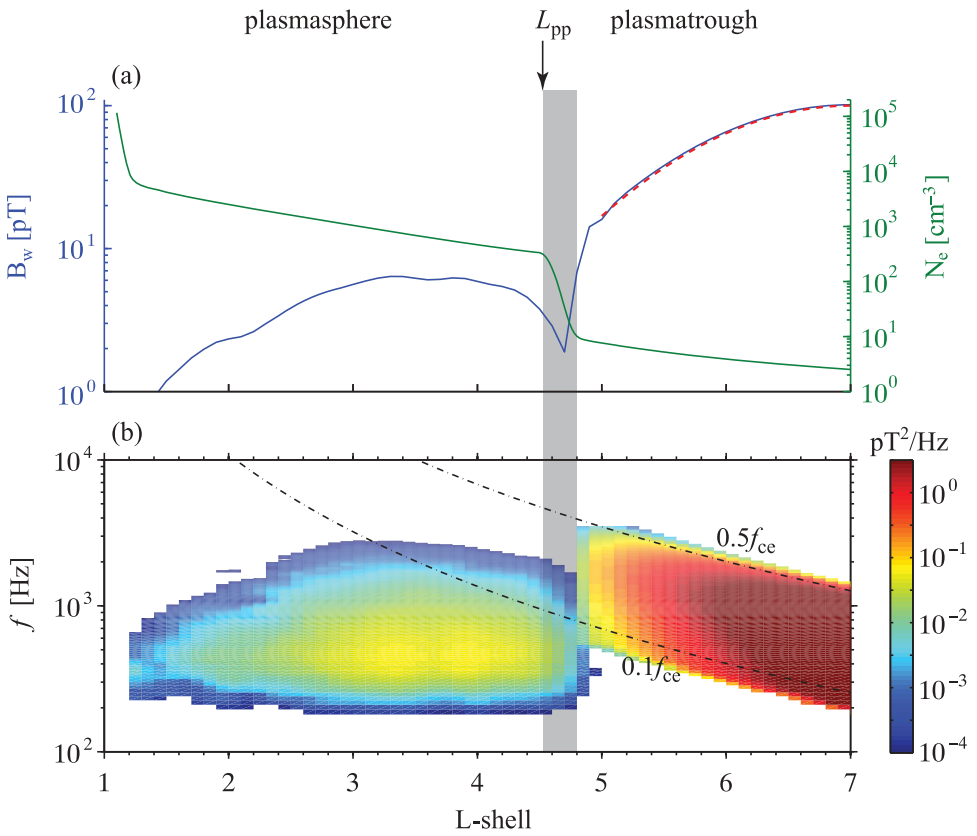

Figure 4. Distribution of wave power as a function of L-shell and frequency on the equatorial plane, representative of MLT = 10. (a) Electron number density delineating the plasmasphere and plasmatrough, separated by the plasmapause at L_{pp} = 4.5 (green line), and band-integrated wave power (blue line). The red dashed line shows the prescribed chorus wave power at $L \geq 5$. (b) Wave power as a function of L-shell and frequency.

is returning valid results, and as expected the blue and red-dashed curves overlap in the chorus source region. The PH integrated values reach a peak value of ~7 pT at $L \sim 3 - 4$, which is lower than average observed storm time values, e.g., 40 pT [*Meredith et al.*, 2004]. The origin of this important discrepancy may be due to a number of approximations in our modeling. First, the average distribution of chorus wave power we have used may be too weak, or be distributed incorrectly in L or ψ. Secondly, we have only included Landau damping in the present model. Any anisotropy of the cyclotron resonant electrons that gain access to the plasmasphere [e.g. *Li et al.*, 2010] will contribute to a modest growth of those waves that propagate across the equator with small wave normal angles [*Church and Thorne*, 1983]. These two possibilities are beyond the scope of the present work but will be examined in future studies.

[26] The distribution shown in Figure 4 can be readily compared to satellite observations. As an example, we have expanded the PH region in Figure 1, and resampled the data onto a uniform L grid. The CRRES results are shown in Figure 5a, in the range $L = 1.5 - 6.5$, and $f = 0.1 - 10$ kHz, and our simulated distribution is shown in Figure 5b on the same L and f scales. In Figures 5a and 5b, the color scale has been adjusted to show only 5 orders of magnitude, and clamped at the upper end of the range at approximately the highest intensities of the PH. Although the CRRES data shows PH on the dayside and has $L_{pp} \sim 4.7$ (similar to the simulation), we have made no attempt to simulate this particular event, so direct comparison needs to be made with caution (particularly since we are comparing E-field measurements from CRRES against our simulated B-field). Nevertheless, there are a number of striking similarities between the simulation and the data. First, the bandwidth of the PH is fairly consistent, extending from $f \sim 0.2$ kHz to a few kHz in Figures 5a and 5b, and diminishing with decreasing L, such that at $L < 2$, the bandwidth is only a few hundred Hz, centered at ~0.3 − 0.4 kHz. Secondly, the PH power in Figures 5a and 5b shows two separate power maxima, separated at roughly $L = 3.7$. This two-zone structure of PH has been observed previously (e.g., *Tsurutani et al.* [1975], albeit at lower L), and is a fairly typical feature in the data [see, e.g., *Meredith et al.*, 2004, Figure 2]. Third, the PH in Figures 5a and 5b is seen to extend all the way from the plasmapause to $L < 2$ as noted above. As a final note, we mention that in our simulation, some of the PH wave power has leaked out of the plasmasphere and appears as a weak additional emission in the region outside the plasmapause, down to $f \sim 0.2$ kHz. This appears to be consistent with the weaker emission below the chorus in the data [e.g., *Cornilleau-Wehrlin et al.*, 1978], although we

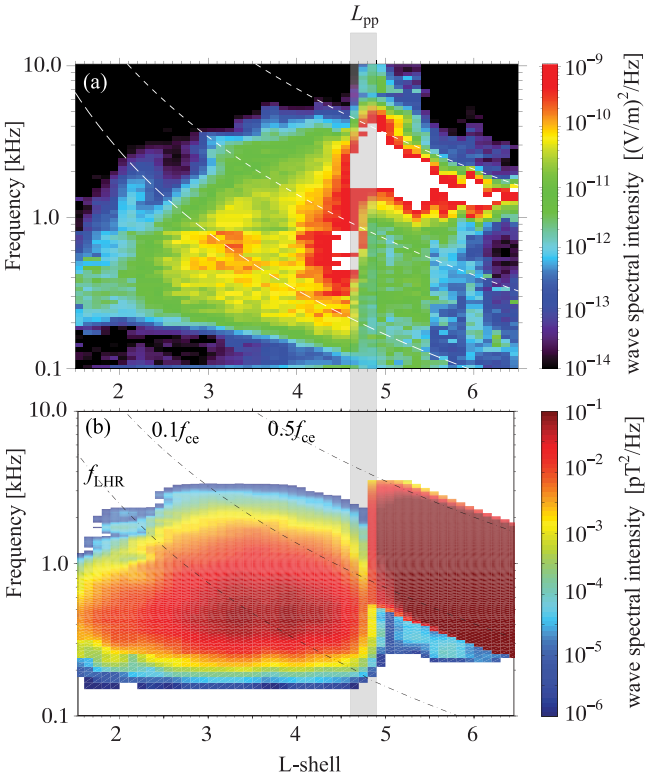

Figure 5. A comparison of PH observation and simulation. (a) The CRRES observation shown in Figure 1, expanded around the region of the hiss emission and resampled onto a uniform-L grid. Intensities above 10^{-9} (V/m)^2/Hz are set to white. (b) The simulated spectrum of the hiss wave shown over the same dynamic range, with values below 10^{-6} pT^2/Hz set to white.

cannot be absolutely certain that the two emissions are the same.

[27] Figure 6 shows the distribution of wave power as a function of L and λ for selected frequencies, i.e., $P_w(L_t, \lambda_t, f_t = 300, 600, 900$ Hz), and again integrated over all wave normal angles ψ_t. Interestingly, in Figures 6a–6c the PH and chorus wave populations appear to be distinct and disconnected from each other, even though it is known (at least in this simulation) that the sole source of the PH lies in the chorus waves. The two zone structure of the PH in L is clearly visible in Figure 6a, and to a lesser degree in Figure 6b, as well as an intensification of the wave power at higher-latitudes which is related to the convergence of the magnetic field lines. This off-equatorial intensification is similar to the peaks observed in statistical distributions [e.g., *Meredith et al.*, 2004, Figure 5]. In comparing all 3 frequency components, it is also apparent that the low frequency component tends to occupy a spatial region that extends all the way to the plasmapause inner edge (dashed line), and perhaps even slightly beyond it, whereas the middle and upper frequency components extend just up to the plasmapause or are contained well within it, respectively.

[28] Figure 7 shows the distribution of wave power within the plasmapshere, as a function of ψ and λ, parameterized by L-shell, i.e., $P_w(L_t = 2 - 4, \lambda_t, \psi_t)$, and integrated over all frequencies. Interestingly, these distributions reveal a consistent structure in ψ and λ, which changes slowly with L. At low L, i.e., $L = 2$, 2.5 the wave power near the equator only shows propagation parallel ($\psi = 0°$) or anti-parallel ($\psi = \pm 180°$) to the field, whereas at high latitudes

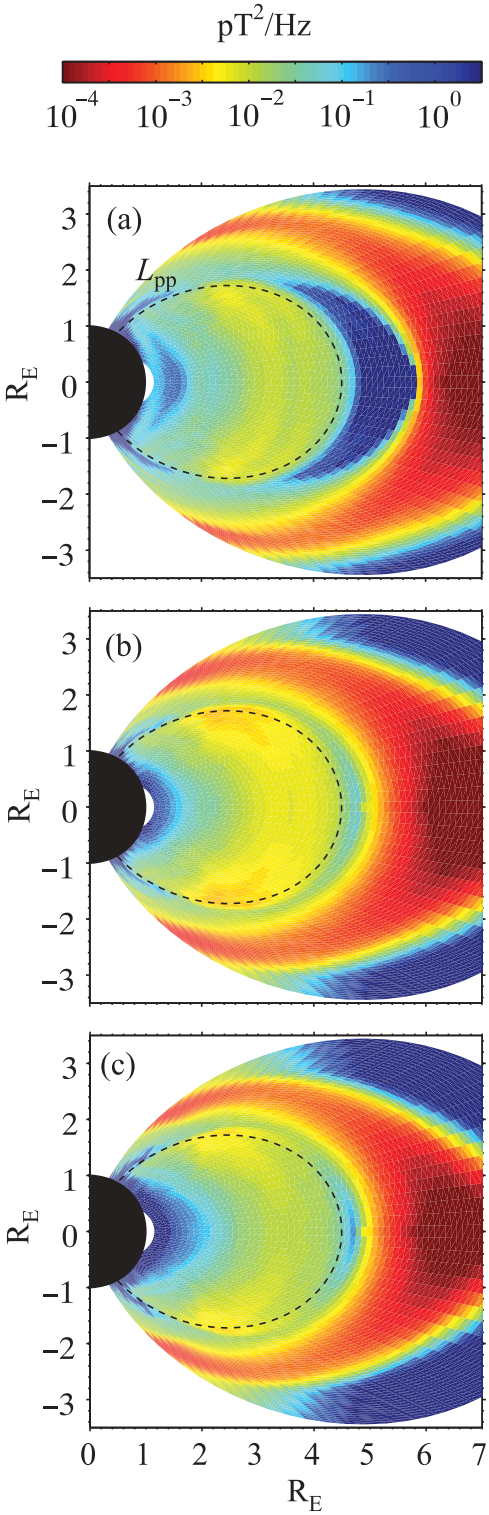

Figure 6. Meridional distribution of wave power for (a) 300 Hz, (b) 600 Hz, and (c) 900 Hz frequency components. The common color bar is shown above, and the dashed lines mark the inner edge of the plasmapause at $L_{pp} = 4.5$.

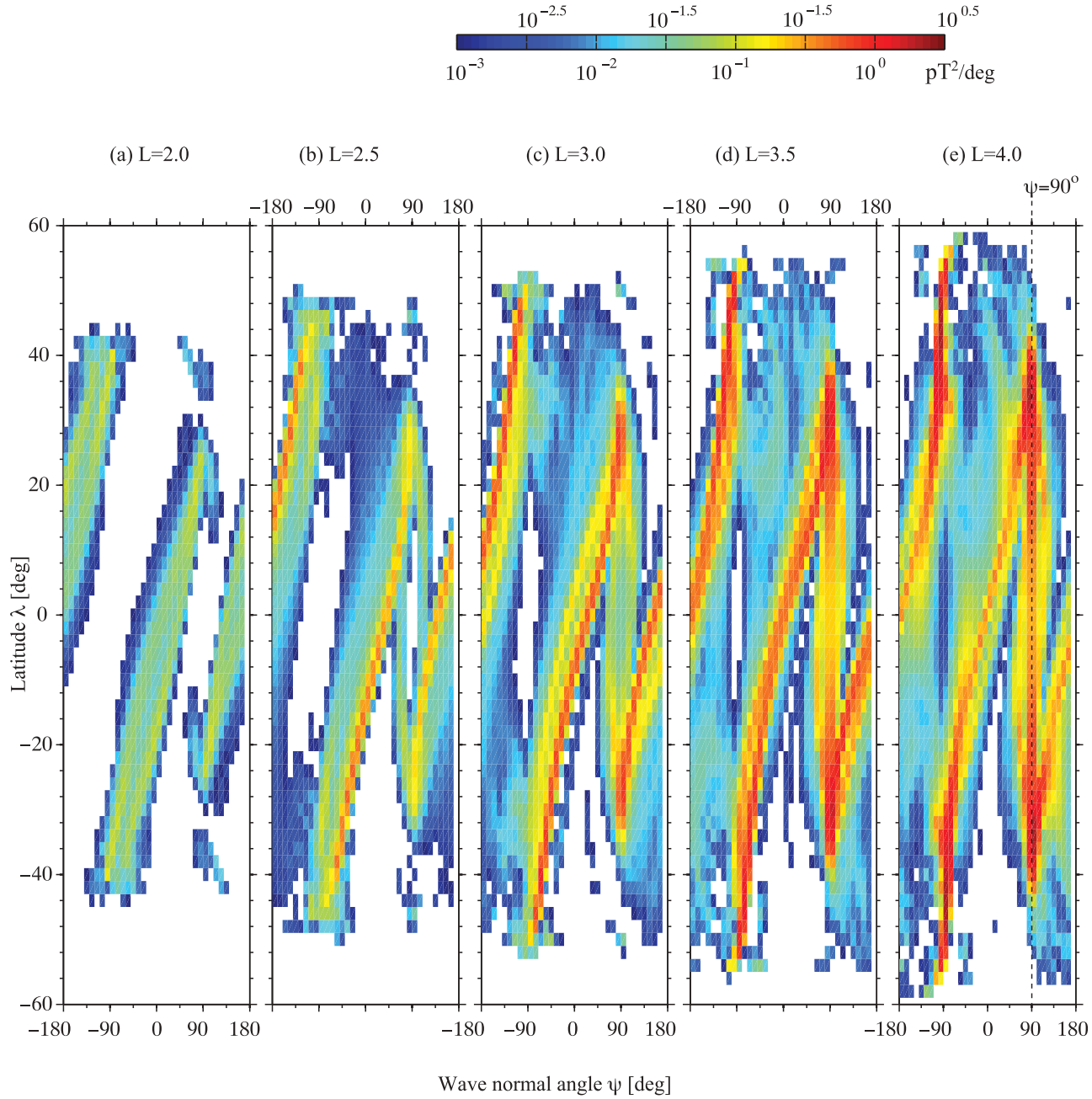

Figure 7. Distribution of wave power as a function of wave normal angle ψ and latitude λ within the plasmapshere for (a) L = 2.0, (b) L = 2.5, (c) L = 3.0, (d) L = 3.5, and (e) L = 4.0.

the wave power only shows propagation perpendicular to the field (ψ = ±90°), and at midlatitudes the wave distribution transitions smoothly from the equatorial to the high-latitude characteristics. The behavior of the wave power can be inferred by examining the individual rays that make up the distribution (e.g., Figure 3) which show that rays cross the equator with small values of ψ, but that at the high latitudes the rays experience magnetospheric reflections (MR) which necessarily result in ψ = ±90°.

[29] On the other hand, at the high L shells (L = 3.5,4) the same behavior is still apparent, but an additional population of waves appears at ψ = 90° at all latitudes. This population results from those rays that have broken out of their cyclical trajectories (e.g., Figure 3f), and have started to magnetospherically reflect back and forth across the equator, at $\psi \sim 90°$ (e.g., Figure 3d), similar to lightning-generated MR whistlers [*Bortnik et al.*, 2003].

[30] At this point, we return to the PH wave normal studies discussed in the introduction, and attempt to interpret these observations in the context of the present model results. All the studies agree that at high latitudes the wave normal angles of PH are predominantly oblique, which is accounted for in our model. Deep inside the plasmapshere, observed wave normal angles are predominantly field aligned [*Santolík et al.*, 2001], whereas closer to the plasmapause, it appeared that the distribution was bimodal [*Hayakawa et al.*,

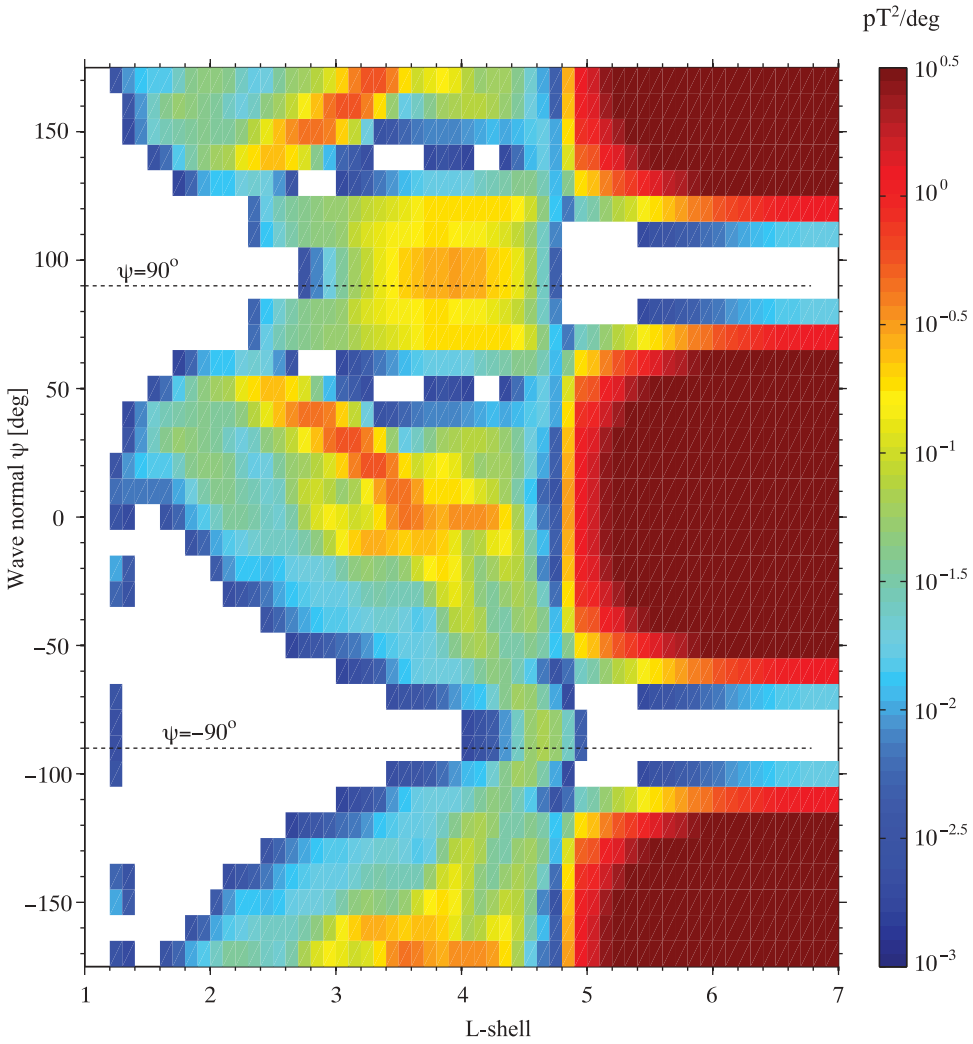

Figure 8. Distribution of wave power as a function of L-shell and wave normal angle ψ along the magnetic equator. Dashed lines indicate perpendicular propagating waves.

1986; *Storey et al.*, 1991; *Hayakawa and Sazhin*, 1992], having one component at low wave normals, and another at high wave normals. This too, is consistent with the results of our model that show the development of a bimodal wave normal distribution close to the plasmapause.

[31] Figure 8 shows the distribution of wave power as a function of L-shell and ψ on the equatorial plane, i.e., $P_w(L_t, \lambda_t = 0°, \psi_t)$, integrated over all f. The saturated wave distribution at $L > 4.8$ represents the chorus source region, whereas the distribution at $L < 4.8$ represents the PH distribution and shows many of the same features that were apparent in Figure 7. At $L = 3.5 - 4.5$ the magnetospherically reflecting distribution of waves shows a maximum at $\psi \sim 90°$, whereas waves on cyclical trajectories have low values of ψ and thus form a bimodal distribution. Interestingly, Figure 8 shows more clearly that at low L-shells ($L < 3$), precisely on the equator, the wave normals do not necessarily peak at $\psi = 0°$, but can shift quite significantly, reaching $\psi \sim 50°$ at $L \sim 2.5$. At still lower L-shells, the equatorial wave normals return to smaller values, albeit at significantly reduced power levels.

[32] As a final means to visualize the distribution of PH wave power, we show in Figure 9 the distribution as a function of ψ and f, parameterized according to L and λ, i.e., $P_w(L_t = 2, 3, 4, \lambda_t = 0°, \pm 20°, f_t, \psi_t)$. Here, we note that the distribution of wave power as a function of ψ is relatively insensitive to f, and shows the same bimodal distributions of wave power near the equator at higher L. These plots exhibit an apparent oddity in that they are meant to be symmetric in the northern and southern hemispheres about the equator (i.e., $\lambda = +20°$ should be similar to $\lambda = -20°$) since we inject our chorus rays symmetrically into the north and south hemisphere from the equatorial chorus source region. The upper and lower rows of Figure 9 are indeed symmetric, but they are symmetric such that $P(\psi > 0°, \lambda = \lambda_0) = P(\pi - \psi, \lambda = -\lambda_0)$ and $P(\psi < 0°, \lambda = \lambda_0) = P(-\pi - \psi, \lambda = -\lambda_0)$. Precisely at the equator (i.e., middle row of Figure 9), this becomes a symmetry about $\psi = \pm 90°$.

4. Discussion and Conclusions

[33] Although we have used a fairly simple model of the plasmasphere, magnetic field, and chorus source region, we

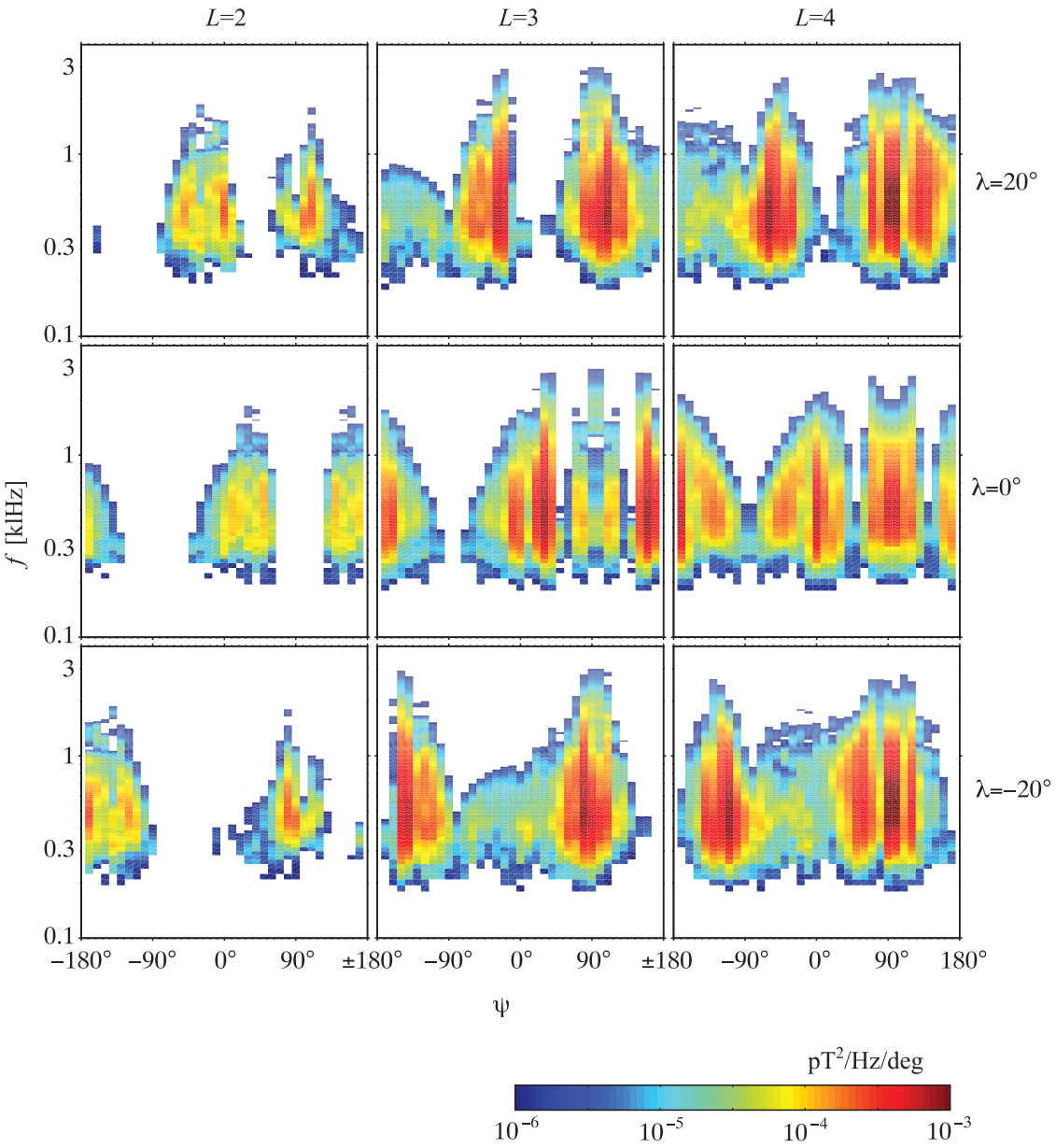

Figure 9. Distribution of wave power as a function of frequency and wave normal angle, at various locations in the plasmasphere. Shown are observation locations at (left) L = 2, (middle) 3, and (right) 4 for (top) λ = +20°, (middle) 0°, and (bottom) −20°.

were able to obtain wave distributions that exhibited many of the same details that are observed in individual satellite events, or in statistical studies. For instance, a comparison of our simulated spectrogram with a single PH event observed on the CRRES satellite showed very similar lower and upper frequency cutoffs, and the same trend for the PH bandwidth that diminished with decreasing L-shell. The spatial extent of both simulation and observation was similar (from the plasmapause to $L < 2$), and even the two zone intensity structure of PH was apparent at roughly the same location.

[34] It may be tempting, in looking at Figures 1 and 5a, to ask whether the PH waves observed just inside the plasmapause could be locally excited by the same unstable particle population that is responsible for exciting the chorus waves just outside the plasmapause, the frequency shift being due to the change in plasma density. Indeed, using 10 keV as a representative (parallel) energy of the plasma sheet particles, and calculating the resonant wave frequency using (1) gives f_{res} = 700 Hz at L = 4.5 (where N_{eq} = 300 cm^{-3}), and f_{res} = 3200 Hz at L = 5 (where N_{eq} = 5 cm^{-3}), in agreement with observation. However, since the growth rates scale roughly as N_{eq}^{-1} (assuming the hot particle density is constant), they will be a factor of ~60 lower inside the plasmasphere than outside, which is probably too low for spontaneous wave emissions, but could still provide modest amplification to existing waves that traverse that region.

[35] As noted above, the simulated intensity of our PH (~7 pT) was somewhat weaker than average observed values (~40 pT [*Meredith et al.*, 2004]) which deserves some discussion. This could be due to a number of factors:

it is possible that our assumed distribution of the chorus source was incorrect, and that a more accurate distribution would give a greater power weighting to those rays that propagate and evolve into PH. Another possibility might have to do with the fact that we have only assumed Landau damping in our model, and neglected cyclotron growth. In reality, a region exists just inside the plasmapause where plasma sheet particles are transported across the plasmapause with sufficient flux and anisotropy [e.g., *Li et al.*, 2010] to lead to cyclotron resonant wave growth of parallel propagating waves. As discussed above, and referring to Figure 2, the cyclotron resonant energies of PH decrease to their lowest values ($E_{res} \sim 10$ keV) close to the plasmapause, and so it is only in this region where we expect that significant growth will take place as described earlier by *Church and Thorne* [1983]. We note that since the rays are on cyclical trajectories, only a modest gain (few dB) is needed at each equatorial traverse to raise the overall power of PH significantly. We also note that in Figure 5a, the largest intensities of PH were found very close to, but still within the plasmapause, consistent with this idea of modest wave growth.

[36] Certain observations have even suggested that PH could be generated spontaneously near the equator within one traverse having an amplification of ~100 − 130 dB [e.g., *Solomon et al.*, 1988; *Cornilleau-Wehrlin et al.*, 1993]. However, it seems that these reported fluxes are far more intense than typical values obtained with larger and more modern data sets [e.g., *Li et al.*, 2010], even when comparing fluxes outside the plasmapause. Moreover, if a few cyclical ray trajectories were to pass through this region (as indicated by the present and past studies [e.g., *Thorne et al.*, 1979; *Church and Thorne*, 1983; *Huang and Goertz*, 1983; *Huang et al.*, 1983; *Bortnik et al.*, 2008, 2009]), then the wave amplitudes would very quickly become implausibly large. It is also possible that inclusion of azimuthal propagation could bring in additional wave power from different local times, although as shown by *Chen et al.* [2009] this would work most effectively in the post-noon region where azimuthal density gradients are largest, and less so in the dawn region where waves tend to stay closely confined to their initial meridians. A final possibility is that an additional source might be contributing power into the PH spectrum, such as chorus generated in off-equatorial minimum-B pockets [*Tsurutani et al.*, 2009], or lightning-generated MR whistlers [e.g., *Draganov et al.*, 1992, 1993; *Bortnik et al.*, 2003]. The first possibility does not seem likely, since minimum-B pockets generally occur at high *L*-shells, and chorus generated therein would likely not reach the plasmapause without significant damping. The second option also does not seem very likely. Since the PH spectrum does not scale with the lower hybrid resonance frequency (as MR whistlers would tend to do), and predominantly field-aligned wave normals are observed deep within the plasmasphere, lightning-generated MR whistlers probably do not represent a major source of PH.

[37] The wave normal distribution of PH showed that at high latitudes, the wave normals are predominantly oblique, but near the equator, the wave normal distribution can be either predominantly field-aligned (lower *L* shells), or be bimodal, having a maximum in the field-aligned direction, and another maximum at very oblique angles, from those rays that have broken out of their cyclical trajectories. This distribution of wave normals seems to reconcile the apparently contradictory observations that have been reported previously, using the WDF technique (see sections 3 and 1). We observe that our calculated PH distribution is somewhat similar to the characteristics often used in diffusion codes near the equator, having a constant amplitude along the field line, with either zero wave normal [e.g., *Li et al.*, 2007; *Summers et al.*, 2007], or some modest spread of wave normals about a constant value, usually zero [e.g., *Lyons et al.*, 1972; *Abel and Thorne*, 1998a, 1998b; *Albert*, 2008]. However, the similarity breaks down at higher latitudes (and near the plasmapause), where our model shows a concentration of power at large wave normal angles. This distinction is expected to lead to large differences in the diffusion rates that have been calculated, particularly for very high energy electrons (e.g., Figure 2), and especially so since particles spend a large portion of their bounce time near the mirror points.

[38] We thus conclude that despite the lower overall intensities of PH in our simulation compared to observations, the simulation results show a remarkable degree of consistency with the observed characteristics of PH, including its spatial extent, frequency cutoffs, bandwidth, two-zone distribution, and wave normal. Thus it appears that the chorus is indeed the dominant source of PH and is sufficient to explain its basic features.

[39] **Acknowledgements.** J.B., L.C., W.L. and R.M.T. would like to gratefully acknowledge the support of the NSF through grant AGS-0840178. We would like to thank Roger Anderson for provision of the CRRES plasma wave data used in this study. N.P.M. and R.B.H. would like to acknowledge support from the Natural Environment Research Council. The research leading to these results has received funding from the European Community's Seventh Framework Programme (FP7/2007-2013) under grant agreement 262468.

[40] Robert Lysak thanks Reinhard Friedel and another reviewer for their assistance in evaluating this paper.

References

Abel, R. W., and R. M. Thorne (1998a), Electron scattering loss in Earth's inner magnetosphere: 1. Dominant physical processes, *J. Geophys. Res.*, *103*, 2385–2396.

Abel, R. W., and R. M. Thorne (1998b), Electron scattering loss in Earth's inner magnetosphere: 2. Sensitivity to model parameters, *J. Geophys. Res.*, *103*, 2397–2408.

Albert, J. M. (1994), Quasi-linear pitch angle diffusion coefficients: Retaining high harmonics, *J. Geophys. Res.*, *99*, 23,741–23,745.

Albert, J. M. (2005), Evaluation of quasi-linear diffusion coefficients for whistler mode waves in a plasma with arbitrary density ratio, *J. Geophys. Res.*, *110*, A03218, doi:10.1029/2004JA010844.

Albert, J. M. (2008), Efficient approximations of quasi-linear diffusion coefficients in the radiation belts, *J. Geophys. Res.*, *113*, A06208, doi:10.1029/2007JA012936.

Bortnik, J., U. S. Inan, and T. F. Bell (2003), Energy distribution and lifetime of magnetospherically reflecting whistlers in the plasmasphere, *J. Geophys. Res.*, *108*(A5), 1199, doi:10.1029/2002JA009316.

Bortnik, J., R. M. Thorne, and N. P. Meredith (2007), Modeling the propagation characteristics of chorus using CRRES suprathermal electron fluxes, *J. Geophys. Res.*, *112*, A08204, doi:10.1029/2006JA012237.

Bortnik J., R. M. Thorne, and N. P. Meredith (2008), The unexpected origin of plasmaspheric hiss from discrete chorus emissions, *Nature*, *452*(7183), 62–66.

Bortnik, J., W. Li, R. M. Thorne, V. Angelopoulos, C. Cully, J. Bonnell, O. Le Contel, and A. Roux (2009), An observation linking the origin of plasmaspheric hiss to discrete chorus emissions, *Science*, *324*(5928), 775–778, doi:10.1126/science.1171273.

Bortnik, J., L. Chen, W. Li, R. Thorne, and R. Horne (2011), Modeling the evolution of chorus waves into plasmaspheric hiss, *J. Geophys. Res.*, *116*, A08221, doi:10.1029/2011JA016499.

Burtis, W. J., and R. A. Helliwell (1969), Banded chorus: A new type of VLF radiation observed in the magnetosphere by OGO 1 and OGO 3, *J. Geophys. Res.*, *74*, 3002–3919, doi:10.1029/JA074i011p03002.

Burtis, W. J., and R. A. Helliwell (1976), Magnetospheric chorus: Occurrence patterns and normalized frequency, *Planet. Space Sci.*, *24*(11), 1007–1007.

Burton, R. K., and R. E. Holzer (1974), The origin and propagation of chorus in the outer magnetosphere, *J. Geophys. Res.*, *79*(7), 1014–1023.

Carpenter, D. L., and R. R. Anderson (1992), An ISEE/whistler model of equatorial electron density in the magnetosphere, *J. Geophys. Res.*, *97*(A2), 1097–1108.

Chan, K. W., and R. E. Holzer (1976), ELF hiss associated with plasma density enhancements in the outer magnetosphere, *J. Geophys. Res.*, *81*, 2267–2274.

Chen, L., J. Bortnik, R. M. Thorne, R. B. Horne, and V. K. Jordanova (2009), Three-dimensional ray tracing of VLF waves in a magnetospheric environment containing a plasmaspheric plume, *Geophys. Res. Lett.*, *36*, L22101, doi:10.1029/2009GL040451.

Church, S. R., and R. M. Thorne (1983), On the origin of plasmaspheric hiss: Ray path integrated amplification, *J. Geophys. Res.*, *88*(A10), 7941–7957.

Cornilleau-Wehrlin, N., R. Gendrin, F. Lefeuvre, M. Parrot, R. Grard, D. Jones, A. Bahnsen, E. Ungstrup, and W. Gibbons (1978), VLF electromagnetic waves observed onboard GEOS-1, *Space Sci. Rev.*, *22*, 371–382.

Cornilleau-Wehrlin, N., J. Solomon, A. Korth, and G. Kremser (1993), Generation mechanism of plasmaspheric ELF/VLF hiss: A statistical study from GEOS 1 data, *J. Geophys. Res.*, *98*(A12), 21,471–21,479.

Denton, R. E., J. Goldstein, and J. D. Menietti (2002), Field line dependence of magnetospheric electron density, *Geophys. Res. Lett.*, *29*(24), 2205, doi:10.1029/2002GL015963.

Draganov, A. B., U. S. Inan, V. S. Sonwalkar, and T. F. Bell (1992), Magnetospherically reflected whistlers as a source of plasmaspheric hiss, *Geophys. Res. Lett.*, *19*(3), 233–236.

Draganov, A. B., U. S. Inan, V. S. Sonwalkar, and T. F. Bell (1993), Whistlers and plasmaspheric hiss: Wave directions and 3-dimensional propagation, *J. Geophys. Res.*, *98*(A7), 11,401–11,410.

Dunckel, N., and R. A. Helliwell (1969), Whistler mode emissions on the OGO 1 satellite, *J. Geophys. Res.*, *74*, 6371–6385.

Glauert, S. A., and R. B. Horne (2005), Calculation of pitch angle and energy diffusion coefficients with the PADIE code, *J. Geophys. Res.*, *110*, A04206, doi:10.1029/2004JA010851.

Goldstein, B. E., and B. T. Tsurutani (1984), Wave normal directions of chorus near the equatorial source region, *J. Geophys. Res.*, *89*(A5), 2789–2810.

Hayakawa, M., and S. S. Sazhin (1992), Mid-latitude and plasmaspheric hiss: A review, *Planet. Space Sci.*, *40*(10), 1325–1338.

Hayakawa, M., Y. Yamanaka, M. Parrot, and F. Lefeuvre (1984), The wave normals of magnetospheric chorus emissions observed onboard GEOS 2, *J. Geophys. Res.*, *89*, 2811–2821.

Hayakawa, M., N. Ohmi, M. Parrot, and F. Lefeuvre (1986), Direction finding of ELF hiss emissions in a detached plasma region of the magnetosphere, *J. Geophys. Res.*, *91*, 135–141.

Hayakawa, M., K. Hattori, S. Shimakura, M. Parrot, and F. Lefeuvre (1990), Direction finding of chorus emissions in the outer magnetosphere and their generation and propagation, *Planet. Space Sci.*, *38*, 135–143, doi:10.1016/0032-0633(90)90012-F.

Huang, C. Y., and C. K. Goertz (1983), Ray-tracing studies and path-integrated gains of ELF unducted whistler-mode waves in the Earth's magnetosphere, *J. Geophys. Res.*, *88*, 6181–6187.

Huang, C. Y., C. K. Goertz, and R. R. Anderson (1983), A theoretical study of plasmaspheric hiss generation, *J. Geophys. Res.*, *88*, 7927–7940.

Kennel, C. (1966), Low-frequency whistler mode, *Phys. Fluids*, *9*, 2190–2202.

Koons, H. (1981), The role of hiss in magnetospheric chorus emissions, *J. Geophys. Res.*, *86*(A8), 6745–6754.

Lam, M. M., R. B. Horne, N. P. Meredith, and S. A. Glauert (2007), Modeling the effects of radial diffusion and plasmaspheric hiss on outer radiation belt electrons, *Geophys. Res. Lett.*, *34*, L20112, doi:10.1029/2007GL031598.

Lauben, D. S., U. S. Inan, T. F. Bell, D. L. Kirchner, G. B. Hospodarsky, and J. S. Pickett (1998), VLF chorus emissions observed by Polar during the January 10, 1997, magnetic cloud, *Geophys. Res. Lett.*, *25*, 2995–2998, doi:10.1029/98GL01425.

Lauben, D. S., U. S. Inan, T. F. Bell, and D. A. Gurnett (2002), Source characteristics of ELF/VLF chorus, *J. Geophys. Res.*, *107*(A12), 1429, doi:10.1029/2000JA003019.

LeDocq, M. J., D. A. Gurnett, and G. B. Hospodarsky (1998), Chorus source locations from VLF Poynting flux measurements with the Polar spacecraft, *Geophys. Res. Lett.*, *25*(21), 4063–4066.

Lefeuvre, F., and R. A. Helliwell (1985), Characterization of the sources of VLF hiss and chorus observed on GEOS 1, *J. Geophys. Res.*, *90*, 6419–6438.

Li, W., Y. Y. Shprits, and R. M. Thorne (2007), Dynamic evolution of energetic outer zone electrons due to wave-particle interactions during storms, *J. Geophys. Res.*, *112*, A10220, doi:10.1029/2007JA012368.

Li, W., R. M. Thorne, V. Angelopoulos, J. Bortnik, C. M. Cully, B. Ni, O. LeContel, A. Roux, U. Auster, and W. Magnes (2009), Global distribution of whistler-mode chorus waves observed on the THEMIS spacecraft, *Geophys. Res. Lett.*, *36*, L09104, doi:10.1029/2009GL037595.

Li, W., R. M. Thorne, J. Bortnik, Y. Nishimura, V. Angelopoulos, L. Chen, J. P. McFadden, and J. W. Bonnell (2010), Global distributions of suprathermal electrons observed on THEMIS and potential mechanisms for access into the plasmasphere, *J. Geophys. Res.*, *115*, A00J10, doi:10.1029/2010JA015687.

Li, W., R. M. Thorne, J. Bortnik, Y. Y. Shprits, Y. Nishimura, V. Angelopoulos, C. Chaston, O. Le Contel, and J. W. Bonnell (2011), Characteristic properties of rising and falling tone chorus waves, *Geophys. Res. Lett.*, *38*, L14103, doi:10.1029/2011GL047925.

Lyons, L. R., and R. M. Thorne (1973), Equilibrium structure of radiation belt electrons, *J. Geophys. Res.*, *78*(13), 2142–2149.

Lyons, L. R., R. M. Thorne, and C. F. Kennel (1972), Pitch-angle diffusion of radiation belt electrons within the plasmasphere, *J. Geophys. Res.*, *77*, 3455–3474.

Means, J. D. (1972), Use of the three-dimensional covariance matrix in analyzing the polarization properties of plane waves, *J. Geophys. Res.*, *77*, 5551–5559.

McPherron, R. L., C. T. Russell, and P. J. Coleman Jr. (1972), Fluctuating magnetic fields in the magnetosphere, II. ULF waves, *Space Sci. Rev.*, *13*, 411–454.

Meredith, N. P., R. B. Horne, and R. R. Anderson (2001), Substorm dependence of chorus amplitudes: Implications for the acceleration of electrons to relativistic energies, *J. Geophys. Res.*, *106*(A7), 13,165–13,178.

Meredith, N. P., R. B. Horne, R. M. Thorne, and R. R. Anderson (2003), Favored regions for chorus-driven electron acceleration to relativistic energies in the Earth's outer radiation belt, *Geophys. Res. Lett.*, *30*(16), 1871, doi:10.1029/2003GL017698.

Meredith, N. P., R. B. Horne, R. M. Thorne, D. Summers, and R. R. Anderson (2004), Substorm dependence of plasmaspheric hiss, *J. Geophys. Res.*, *109*, A06209, doi:10.1029/2004JA010387.

Meredith, N. P., R. B. Horne, M. A. Clilverd, D. Horsfall, R. M. Thorne, and R. R. Anderson (2006a), Origins of plasmaspheric hiss, *J. Geophys. Res.*, *111*, A09217, doi:10.1029/2006JA011707.

Meredith, N. P., R. B. Horne, S. A. Glauert, R. M. Thorne, D. Summers, J. M. Albert, and R. R. Anderson (2006b), Energetic outer zone electron loss timescales during low geomagnetic activity, *J. Geophys. Res.*, *111*, A05212, doi:10.1029/2005JA011516.

Meredith, N. P., R. B. Horne, S. Glauert, and R. R. Anderson (2007), Slot region electron loss timescales due to plasmaspheric hiss and lightning generated whistlers, *J. Geophys. Res.*, *112*, A08214, doi:10.1029/2007JA012413.

Meredith, N. P., R. B. Horne, S. A. Glauert, D. N. Baker, S. G. Kanekal, and J. M. Albert (2009), Relativistic electron loss timescales in the slot region, *J. Geophys. Res.*, *114*, A03222, doi:10.1029/2008JA013889.

Parrot, M., and F. Lefeuvre (1986), Statistical study of the propagation characteristics of ELF hiss observed on GEOS-1, inside and outside the plasmasphere, *Ann. Geophys.*, *4*, 363.

Parrot, M., O. Santolík, N. Cornilleau-Wehrlin, M. Maksimovic, and C. Harvey (2003), Source location of chorus emissions observed by Cluster, *Ann. Geophys.*, *21*, 473–480.

Russell, C. T., R. E. Holzer, and E. J. Smith (1969), OGO 3 observations of ELF noise in the magnetosphere: 1. Spatial extent and frequency of occurrence, *J. Geophys. Res.*, *74*, 755–777.

Samson, J. C. (1973), Descriptions of the polarization states of vector processes: Applications to ULF magnetic fields, *Geophys. J. R. Astron. Soc.*, *34*, 403–419.

Samson, J. C., and J. V. Olsen (1980), Some comments on the descriptions of the polarization states of waves, *Geophys. J. R. Astron. Soc.*, *61*, 115–129.

Santolík, O., and M. Parrot (1999), Case studies on the wave propagation and polarization of ELF emissions observed by Freja around the local proton gyrofrequency, *J. Geophys. Res.*, *104*(A2), 2459–2475.

Santolík, O., and M. Parrot (2000), Application of wave distribution function methods to an ELF hiss event at high latitudes, *J. Geophys. Res.*, *105*, 18,885–18,894.

Santolík, O., M. Parrot, L. R. O. Storey, J. S. Picket, and D. A. Gurnett (2001), Propagation analysis of plasmaspheric hiss using Polar PWI measurements, *Geophys. Res. Lett.*, *28*(6), 1127–1130.

Santolík, O., M. Parrot, and F. Lefeuvre (2003a), Singular value decomposition methods for wave propagation analysis, *Radio Sci.*, *38*(1), 1010, doi:10.1029/2000RS002523.

Santolík, O., D. A. Gurnett, J. S. Pickett, M. Parrot, and N. Cornilleau-Wehrlin (2003b), Spatio-temporal structure of storm-time chorus, *J. Geophys. Res. 108*(A7), 1278, doi:10.1029/2002JA009791.

Santolík, O., D. A. Gurnett, J. S. Pickett, M. Parrot, and N. Cornilleau-Wehrlin (2005a), Central position of the source region of storm-time chorus, *Planet. Space Sci.*, *53*(1–3), 299–305, doi:10.1016/j.pss.2004.09.056.

Santolík, O., E. Macusova, K. H. Yearby, N. Cornilleau-Wehrlin, and H. S. C. K. Alleyne (2005b), Radial variation of whistler-mode chorus: First results from the STAFF/DWP instrument onboard the Double Star TC 1 spacecraft, *Ann. Geophys.*, *23*, 2937–2942.

Santolík, O., J. Chum, M. Parrot, D. A. Gurnett, J. S. Pickett, and N. Cornilleau-Wehrlin (2006), Propagation of whistler mode chorus to low altitudes: Spacecraft observations of structured ELF hiss, *J. Geophys. Res.*, *111*, A10208, doi:10.1029/2005JA011462.

Santolík, O., D. A. Gurnett, J. S. Pickett, J. Chum, and N. Cornilleau-Wehrlin (2009), Oblique propagation of whistler mode waves in the chorus source region, *J. Geophys. Res.*, *114*, A00F03, doi:10.1029/2009JA014586.

Smith, E. J., A. M. A. Frandsen, B. T. Tsurutani, R. M. Thorne, and K. W. Chan (1974), Plasmaspheric hiss intensity variations during magnetic storms, *J. Geophys. Res.*, *79*, 2507–2510.

Solomon, J., N. Cornilleau-Wehrlin, A. Korth, and G. Kremser (1988), An experimental study of ELF/VLF hiss generation in the Earth's magnetosphere, *J. Geophys. Res.*, *93*(A3), 1839–1847.

Storey, L. R. O., and F. Lefeuvre (1974), Theory for the interpretation of measurements of a random electromagnetic wave field in space, *Space Res.*, *14*, 381–386.

Storey, L. R. O., and F. Lefeuvre (1979), The analysis of 6-component measurement of a random electromagnetic wave field in a magnetoplasma, 1, The direct problem, *Geophys. J. R. Astron. Soc.*, *56*, 255–270.

Storey, L. R. O., and F. Lefeuvre (1980), The analysis of 6-component measurement of a random electromagnetic wave field in a magnetoplasma, 2, The integration kernels, *Geophys. J. R. Astron. Soc.*, *62*, 173–194.

Storey, L. R. O., F. Lefeuvre, M. Parrot, L. Cairo, and R. Anderson (1991), Initial survey of the wave distribution functions for plasmaspheric hiss observed by ISEE 1, *J. Geophys. Res.*, *96*, 19,469–19,489.

Summers, D., B. Ni, and N. P. Meredith (2007), Timescales for radiation belt electron acceleration and loss due to resonant wave particle interactions: 2. Evaluation for VLF chorus, ELF hiss, and EMIC waves, *J. Geophys. Res.*, *112*, A04207, doi:10.1029/2006JA011993.

Summers, D., B. Ni, N. P. Meredith, R. B. Horne, R. M. Thorne, M. B. Moldwin, and R. R. Anderson (2008), Electron scattering by whistler-mode ELF hiss in plasmaspheric plumes, *J. Geophys. Res.*, *113*, A04219, doi:10.1029/2007JA012678.

Taylor, W. W. L., and D. A. Gurnett (1968), Morphology of VLF emissions observed with the Injun 3 satellite, *J. Geophys. Res.*, *73*(17), 5615–5626, doi:10.1029/JA073i017p05615.

Thorne, R. M., E. J. Smith, R. K. Burton, and R. E. Holzer (1973), Plasmaspheric hiss, *J. Geophys. Res.*, *78*, 1581–1595.

Thorne, R. M., E. J. Smith, K. J. Fiske, and S. R. Church (1974), Intensity variation of ELF hiss and chorus driving isolated substorms, *Geophys. Res. Lett.*, *1*, 193–196.

Thorne, R. M., S. R. Church, W. J. Malloy, and B. T. Tsurutani (1977), The local time variation of ELF emissions during periods of substorm activity, *J. Geophys. Res.*, *82*, 1585–1590.

Thorne, R. M., S. R. Church, and D. J. Gorney (1979), On the origin of plasmaspheric hiss: The importance of wave propagation and the plasmapause, *J. Geophys. Res.*, *84*, 5241–5247.

Tsurutani, B. T., E. J. Smith, and R. M. Thorne (1975), Electromagnetic hiss and relativistic electron losses in the inner zone, *J. Geophys. Res.*, *80*(4), 600–607, doi:10.1029/JA080i004p00600.

Tsurutani, B. T., O. P. Verkhoglyadova, G. S. Lakhina, and S. Yagitani (2009), Properties of dayside outer zone chorus during HILDCAA events: Loss of energetic electrons, *J. Geophys. Res.*, *114*, A03207, doi:10.1029/2008JA013353.

J. Bortnik, L. Chen, W. Li, and R. M. Thorne, Department of Atmospheric and Oceanic Sciences, University of California, Los Angeles, CA 90095-1565, USA. (jbortnik@atmos.ucla.edu; clj@atmos.ucla.edu; moonli@atmos.ucla.edu; rmt@atmos.ucla.edu)

R. B. Horne and N. P. Meredith, British Antarctic Survey, Madingley Road, Cambridge CB3 0ET, UK. (rh@bas.ac.uk; nmer@bas.ac.uk)